Numerical Simulations of Island Wakes Downstream Green Island, Taiwan Due to Passing of Kuroshio

Shin-Jye Liang*, Sheng-Lin Lin and Li-Te Chang
Department of Marine Environmental Informatics
National Taiwan Ocean University
2 Pei-Ning Road, Keelung 20224, Taiwan
*sjliang@ntou.edu.tw

***Abstract*—Kuroshio-induced island wake downstream the Green Island, Taiwan is studied using satellite imagery and a depth-averaged shallow-water model. Spatial-temporal scales, such as aspect ratio, dimensionless width, and Strouhal number as well as propagation speed of the vortices are quantified for Reynolds number 100, 200, and 500, respectively. It is found that the aspect ratio is between 1.76 and 2.72 obtained from satellite images and between 3.50 and 3.72 from numerical simulations. The dimensionless width is in the range of 1.84 and 1.92 from satellite images, and 1.29 and 1.33 from numerical modelling. The Strouhal number is between 0.17 and 0.20 from numerical simulations. Computed results are compared with theory, available satellite imagery, and *in-situ* measurements, and show reasonable agreement. Magnitude of the propagation speed of the vortices is found to be the same order as that of the Kuroshio, implying the nonlinearity as well as interactions of vortices and the Kuroshio are strong. Coriolis force does affect the free-surface distribution, however, its effect on vortices and flow field is insignificant.**

Keywords*—Kuroshio; island wake; vortex shedding; spatial-temporal scales; satellite imagery

I. INTRODUCTION

For flow past a circular cylinder the presence or absence of wake is determined by the importance of non-linearity in the flow compared to viscous friction. In non-rotating flow, the form of the wake is dictated by the Reynolds number $Re = u_\infty L_r / \nu_t$, where u_∞, L_r and ν_t are the representative velocity, length, and eddy viscosity, respectively. At $Re < 46 \pm 1$, flow past the bluff obstacle exhibits a steady separated flows; As $Re \geq 46 \pm 1$, flow becomes periodic with detachment of the free shear layer and the consequent shedding of vortices [1]. The periodic phenomenon is referred to as the vortex shedding, while the anti-symmetric wake flow pattern is referred to as the von Kármán vortex streets. The phenomenon of vortex shedding behind bluff bodies has long been of interest to the fluid dynamics community and has been extensively studied by many researchers [2-4]. Many flows of engineering interest produce the phenomena of vortex shedding and the associated structural response. Applications include marine structures, underwater acoustics, civil and wind engineering.

Vortex streets occur frequently in the atmosphere and oceans [5, 6]. The Kuroshio, a western boundary current of the Pacific, originates from the North Equatorial Current and flows northwards to the east of Taiwan. The pathway of the Kuroshio parallels to the east shoreline of Taiwan. Its width is about 100-150 km. The climatology of the Kuroshio velocity from *in-situ* measurements reveals that the Green Island is approximately located in the mainstream of the energetic Kuroshio passing and acts as an obstacle in the stream. The speed of the Kuroshio is about 1.0 m/s on top layer (0 ~ -200 m), 0.5 m/s on the middle layer (-200 m ~ -400 m), and 0.3 m/s on the bottom layer (-400 m ~ -700 m), respectively, according to the field measurements [7]. The influence range of the Kuroshio is up to -800 m; Water below -800 m is basically motionless.

The Green Island locates at 22°35′N, 121°28′E, 40 km off the southeast coast of Taiwan. Fig. 1(a) illustrates the location of Green Island and water depth of the adjacent sea waters. Water depth of the study area, shown in Fig. 1(b), varies from -50 m to -4,000 m, and the average depth is about -2,000 m. The island wakes induce the upwelling and enhance the nitrate concentration in the upper ocean. This kind of phenomenon is often captured by satellite imagery [8] and field measurement [9].

Mesoscale eddies with radius scale O(100 km) are more often studied and better understood because the resolution of satellite altimetry [10]. While small island eddies with radius scale O(10 km), like the island wake downstream Green Island due to passing of the Kuroshio, are less investigated. Simulation of an idealized circular shaped Green island with diameter (D) equal to 5 km and Re = 100 has been conducted and reported in [11]. In this study, the real geometry of Green Island is used. Effects of eddy viscosity and Coriolis force on eddy properties are investigated. Spatial scales (aspect ratio between cross-street and along-street spacing of these vortices), temporal scale (period of the vortices), and propagation speed of these vortices are computed and compared with satellite imagery and other research results.

II. FIELD MEASUREMENTS AND SATELLITE DATA

Vortex streets in the oceans or the atmosphere are often seen on satellite imagery [5, 12]. Fig. 2 illustrates a schematic diagram of flow past a circular island with diameter D and its von Kármán vortex street showing the along-street distance

978-0-933957-40-4 ©2013 MTS

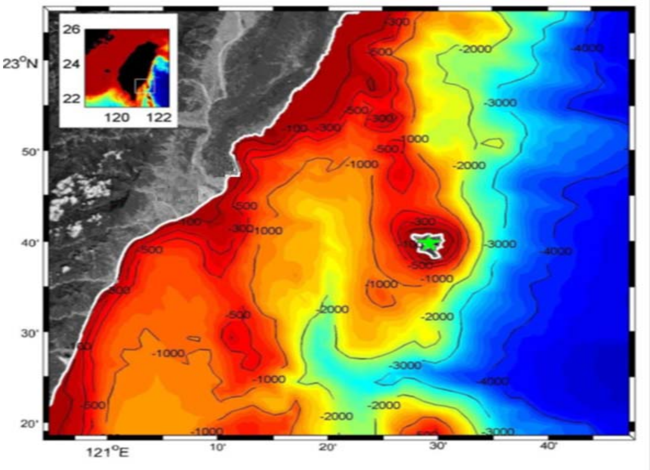

(a)

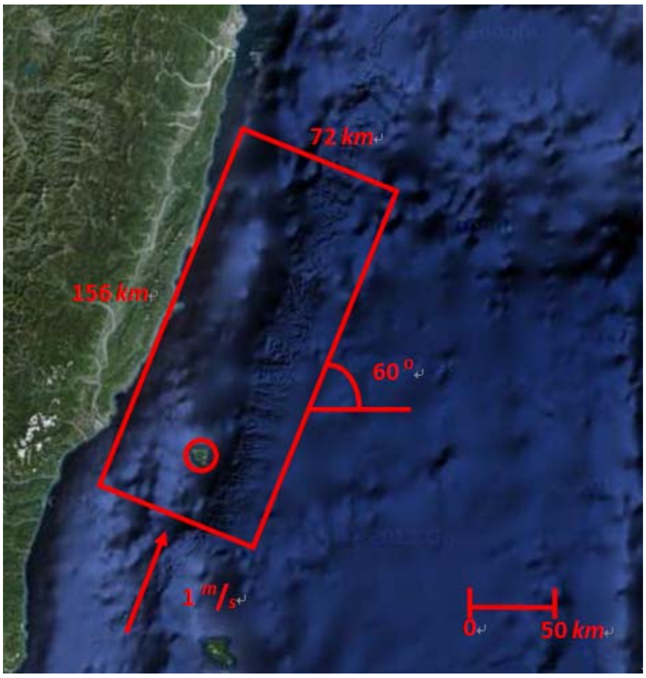

(b)

Fig. 1. (a) Location of Green Island and water depth of the adjacent sea waters, and (b) study area marked by the red rectangle.

and the cross-street distance between two like-rotating vortices. The aspect ratio (a/b) and dimensionless width (b/D) are typical spatial dimensions of vortices. The aspect ratio of vortex streets has been studied extensively in both the atmosphere and laboratory. Laboratory studies yielded value 1.92-3.57 depending on the shape of the body, flow characteristics, and distance downstream. The aspect ratio has a value of 3.57 for the inviscid theory [13], and atmospheric value of 1.67-2.63 from satellite images of the Aleutian chain [14], and 2.00-2.86 from RADARSAT SAR images of Herbert Island [5]. The dimensionless width (b/D) has been studied less extensively, as illustrated in Fig. 2. Remotely sensed imagery usually shows a diverged vortex street in the lee of the island, depicted in Fig. 2(b), which makes the definition of b not unique. Reference [15] stated that it approximates 1.0 for island wakes while [16] reported a value of 1.2 for a bluff body laboratory flow.

Fig. 3(a) shows a synoptic of measured velocity vectors at -19 m and temperature field at -1 m [9]. A recirculation wake followed by a wavy tail exists. The recirculation covers an area about 1-2 times of the Green Island with weak surface current speeds ranging from 0.2 to 0.5 m/s.

Fig. 3(b) shows an oceanic vortex street observed by an ERS (European remote sensing satellite) SAR (synthetic aperture radar) image taken on 29 March 1999. The coverage area of the satellite image is depicted on the top left corner of the inserted figure and landmark of the Green Island is marked, as well. With a spatial resolution of 25 m of the SAR image, meandering disturbances and well-organized oceanic vortex streets are clearly seen over a distance of about 40 km in the lee of the island. The streamwise (a) and transversal length (b) of the vortices determined from the image are 25.4-30.0 km and 9.2-11.2 km, respectively, resulting average value of a = 27.7 km, b = 10.2 km, a/b = 2.72, and b/L_r = 1.84.

Island wake can be identified not only by the high-resolution SAR imagery, but also by the satellite ocean color imagery. An image of MODIS (Moderate Resolution Imaging Spectroradiometer) onboard the Aqua satellite taken on 30 July 2003, see Fig. 3(c), also shows the vortex street over a distance of about 39 km in the lee of Green Island. A pair of eddy-like patterns are seen on the true color MODIS with a spatial resolution of 500 m. The streamwise and transversal lengths of the vortices are 17.1-18.6 km and 9.6-10.7 km, respectively, resulting average value of a = 17.9 km, b = 10.2 km, a/b = 1.76, and b/L_r = 1.92.

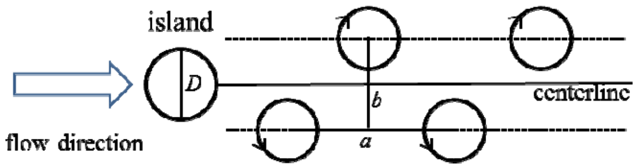

(a)

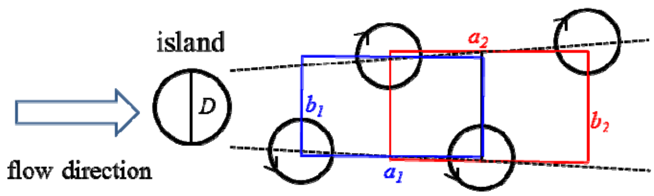

(b)

Fig. 2. A schematic diagram of flow past a circular island with diameter D, and its von Kármán vortex street showing the along-street distance "a" and the cross-street distance "b" between two like-rotating vortices: (a) idealized vortex street for constrained channel flows, and (b) observed vortex street for open ocean flows.

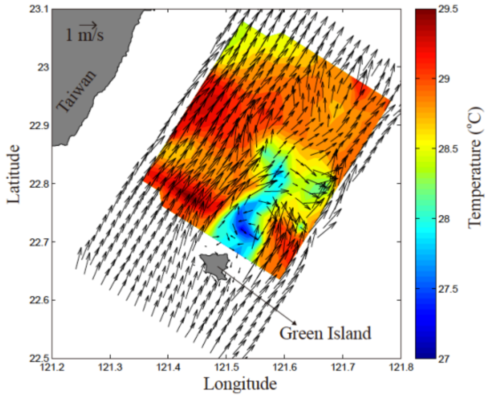

(a)

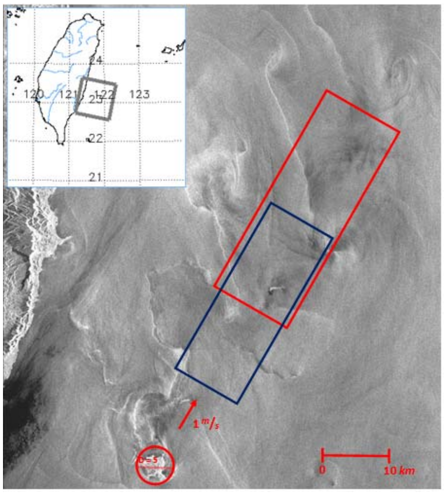

(b)

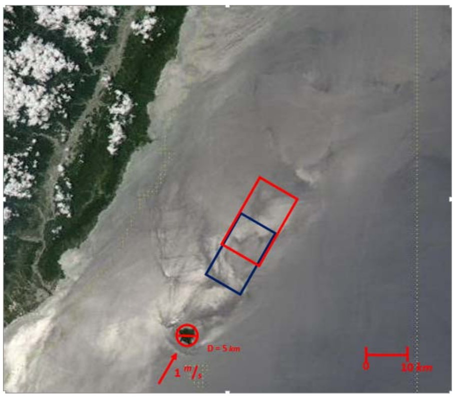

(c)

Fig. 3. (a) A synoptic of measured velocity vectors at -19 m and temperature field at -1 m, respectively [9]. A von Kármán vortex street downstream Green Island, Taiwan from (b) SAR satellite image taken on 29 March 1999, and (c) MODIS image taken on 30 July 2003, respectively. Space dimension of vortices, such as the aspect ratio (a/b) and dimensionless width (b/Lr), is also shown.

III. Shallow-Water Equations and Numerical Method

Shallow-water equations (SWEs) which describes motion of the fluid and space-time least-squares finite-element method (LSFEM) used to solve SWEs are presented in this section.

A. Shallow-Water Equations

To simulate the Green Island wake, a numerical model based on the shallow water equations (SWEs) is applied [11]. SWEs are the simple form of the equations of motion that can be used to describe the horizontal structure of an ocean dynamics. Depth-averaged SWEs is derived from equation of three-dimensional mass and momentum conservation based upon assumption of incompressibility of water, hydrostatic pressure, and a sufficiently small channel slope [17-19]. The two-dimensional viscous SWEs expressed in a non-conservative form read

$$
\begin{aligned}
&\frac{\partial \eta}{\partial t}+\frac{\partial}{\partial x}\left[(H+\eta)u\right]+\frac{\partial}{\partial y}\left[(H+\eta)v\right]=0\\
&\frac{\partial u}{\partial t}+u\frac{\partial u}{\partial x}+v\frac{\partial u}{\partial y}+g\frac{\partial \eta}{\partial x}-fv\\
&=-g\frac{\partial Z_b}{\partial x}+\frac{\rho v_t}{h}\left[2\frac{\partial (hu)}{\partial x}+\left(\frac{\partial (hv)}{\partial x}+\frac{\partial (\rho u)}{\partial y}\right)\right]\\
&\frac{\partial v}{\partial t}+u\frac{\partial v}{\partial x}+v\frac{\partial v}{\partial y}+g\frac{\partial \eta}{\partial y}+fu\\
&=-g\frac{\partial Z_b}{\partial y}+\frac{\rho v_t}{h}\left[\left(\frac{\partial (hv)}{\partial x}+\frac{\partial (\rho u)}{\partial y}\right)+2\frac{\partial (hv)}{\partial y}\right]
\end{aligned}
\tag{1}
$$

where η is the free water surface, H and h are the still water depth and total water depth, u and v are x- and y-component velocity, f is the Coriolis parameter, g is the gravity acceleration, Z_b is the bottom height, v_t is the eddy viscosity, x and y refer the Cartesian coordinates, t is the time, respectively.

Treatment of the open boundary is essential for the success of wave/flow simulations. A simplified 2D open boundary condition introduced in [20] is employed

$$
\frac{\partial \eta}{\partial t}+c\left(k_x\frac{\partial \eta}{\partial x}+k_y\frac{\partial \eta}{\partial y}\right)=0 \tag{2}
$$

where c is the local wave speed, approximated by $\sqrt{gh}$; (k_x, k_y) are the main wave direction along the open boundary, and determined by

$$
k_x=\begin{cases}
\dfrac{\partial \eta}{\partial x}\Big/\sqrt{\left(\dfrac{\partial \eta}{\partial x}\right)^2+\left(\dfrac{\partial \eta}{\partial y}\right)^2} & \text{for } \dfrac{\partial \eta}{\partial x}\geq 0\\[2ex]
-\dfrac{\partial \eta}{\partial x}\Big/\sqrt{\left(\dfrac{\partial \eta}{\partial x}\right)^2+\left(\dfrac{\partial \eta}{\partial y}\right)^2} & \text{for } \dfrac{\partial \eta}{\partial x}< 0
\end{cases}
\tag{3a}
$$

and

$$
k_y = \begin{cases} \dfrac{\partial \eta}{\partial y} / \sqrt{\left(\dfrac{\partial \eta}{\partial x}\right)^2 + \left(\dfrac{\partial \eta}{\partial y}\right)^2} & \text{for } \dfrac{\partial \eta}{\partial y} \geq 0 \\ -\dfrac{\partial \eta}{\partial y} / \sqrt{\left(\dfrac{\partial \eta}{\partial x}\right)^2 + \left(\dfrac{\partial \eta}{\partial y}\right)^2} & \text{for } \dfrac{\partial \eta}{\partial y} < 0 \end{cases} \tag{3b}
$$

B. Space-Time Least-Squares Finite-Element Method

We use 1D shallow-water equations (SWE) to elucidate the formulation of space-time least-squares finite-element method. 1D SWE reads

$$
\begin{cases} \dfrac{\partial \eta}{\partial t} + \dfrac{\partial}{\partial x}\left[(H+\eta)u\right] = 0 \\ \dfrac{\partial u}{\partial t} + u\dfrac{\partial u}{\partial x} + g\dfrac{\partial \eta}{\partial x} = -g\dfrac{\partial b}{\partial x} + T_x \end{cases} \tag{4}
$$

Equation (4) is first linearized by Newton's method

$$
\begin{cases} \dfrac{\partial \eta}{\partial t} + H\dfrac{\partial u}{\partial x} + u\dfrac{\partial d}{\partial x} + \dfrac{\partial}{\partial x}(\tilde{\eta}u + \eta\tilde{u} - \tilde{\eta}\tilde{u}) = 0 \\ \dfrac{\partial u}{\partial t} + \left(\tilde{u}\dfrac{\partial u}{\partial x} + u\dfrac{\partial \tilde{u}}{\partial x} - \tilde{u}\dfrac{\partial \tilde{u}}{\partial x}\right) + g\dfrac{\partial \eta}{\partial x} = -g\dfrac{\partial b}{\partial x} + T_x \end{cases} \tag{5}
$$

where "~" represents value from previous iteration or time step.

In space-time finite-element method, the unknowns ($\underset{\sim}{u} = \{\eta, u\}^T$) are approximated by polynomial interpolations

$$
\begin{Bmatrix} \eta(x,t) \\ u(x,t) \end{Bmatrix} = \begin{bmatrix} M(x)N(t) & \\ & M(x)N(t) \end{bmatrix} \begin{Bmatrix} \eta \\ u \end{Bmatrix} \tag{6}
$$

where $M(x)$ and $N(t)$ are space and time interpolation function, respectively. Substituted approximations (6) into (5), residuals can be obtained

$$
\begin{aligned} \begin{Bmatrix} R_\eta^e \\ R_u^e \end{Bmatrix} = &\begin{bmatrix} \tilde{u}_x MN_1 + MN_1' + \tilde{u}M'N_1 & (\tilde{\eta}_x + H)M\,N_1 + (H+\tilde{\eta})M'N_1 \\ gM'N_1 & \tilde{u}_x M\,N_1 + M\,N_1' + \tilde{u}M'N_1 \end{bmatrix} \begin{Bmatrix} \eta \\ u \end{Bmatrix}^n \\ &+ \begin{bmatrix} \tilde{u}_x MN_2 + MN_2' + \tilde{u}M'N_2 & (\tilde{\eta}_x + H)M\,N_2 + (H+\tilde{\eta})M'N_2 \\ gM'N_2 & \tilde{u}_x M\,N_2 + M\,N_2' + \tilde{u}M'N_2 \end{bmatrix} \begin{Bmatrix} \eta \\ u \end{Bmatrix}^{n+1} \\ &+ \begin{Bmatrix} 0 \\ g\dfrac{\partial b}{\partial x} - \tilde{T}_x \end{Bmatrix} \end{aligned} \tag{7}
$$

Note that piecewise linear interpolation function for time is used, where subscripts "1" and "2" denote number of local nodes, and superscripts "n" and "n+1" denote value of the space-time element at $t = t_n$ and $t_n + 1$, respectively. The least-squares functional and its minimization principle are then constructed

$$
\text{minimize} \int_{\Omega_{xt}} R^2 d\Omega \tag{8}
$$

where Ω_{xt} is the space-time domain considered. The above equation is equivalent to

$$
\int_{\Omega_{xt}} \left\{\frac{\partial R}{\partial \underset{\sim}{u}}\right\} R d\Omega = 0 \tag{9}
$$

Details of the space-time finite-element formulation can be found in [21-25].

IV. NUMERICAL RESULTS AND DISCUSSIONS

Kuroshio-induced vortices of island wake downstream the Green Island, Taiwan is simulated. Satellite imagery and simulation of Green island vortices with Re = 100, 200, and 500, respectively, are presented and discussed.

The study area of simulation is 72 km x 156 km in transversal and streamwise direction, respectively, as shown in Fig. 1(b). The Kuroshio with uniform speed $u_\infty = 1.0$ m/s and an angle 60^o to east enters the computational domain from southwest, and flows downstream to northeast. The representative length of the Green Island $L_r = 5$ km and eddy viscosity $\nu_t = 50\ m^2/s$, therefore, the corresponding Re = 100.

Fig. 4(a) depicts the computational meshes used, total 20,080 nodes and 39,885 triangles. Finer meshes are employed near the Island region, shown in Fig. 4(b), since significant change of flow and wave field in that area is expected. Δt = 90 s is used in computations. Flow starts with a cold condition, i.e. the fluid is at rest initially. It takes a period of transition for flow to develop and reach a periodic state.

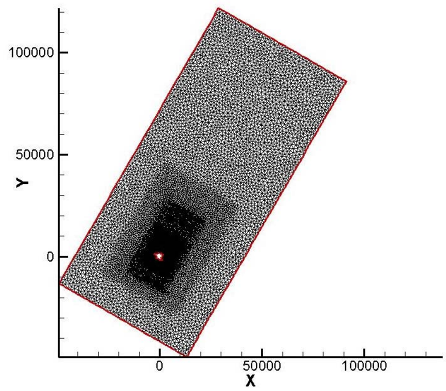

(a)

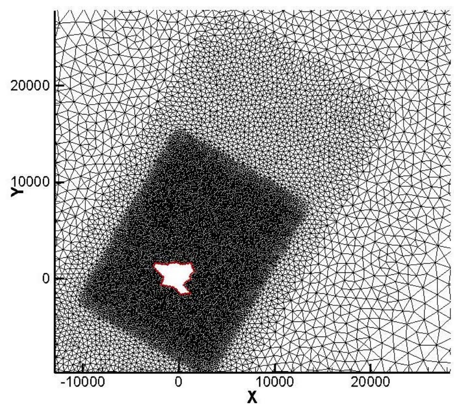

(b)

Fig. 4. Computational meshes, total 20,080 nodes and 39,885 triangles, used: (a) Global view and (b) Close-up local view, respectively.

Fig. 5 illustrates the geometry effect on the island wakes. Fig. 5(a) depicts the streamlines around the idealized circular Green island with diameter D = 5 km, while Fig. 5(b) shows the streamlines around the real shaped Green island. As can be seen, the streamlines are similar for both cases, especially for region about two diameters downstream the island. However, streamlines close to the island are different. There is a persistent small recirculation in the southeastern of the island due to corner there, see Fig. 5(b).

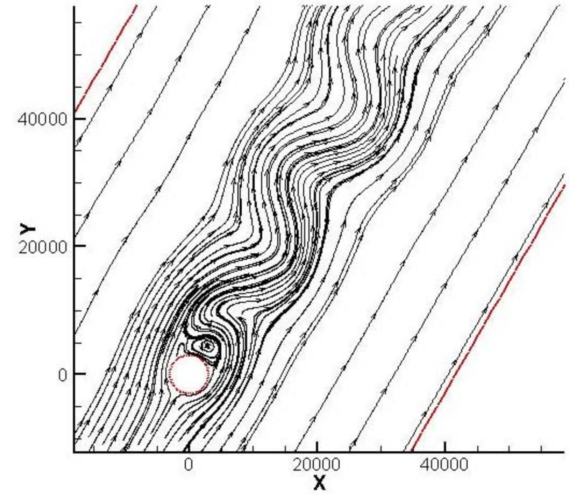

(a)

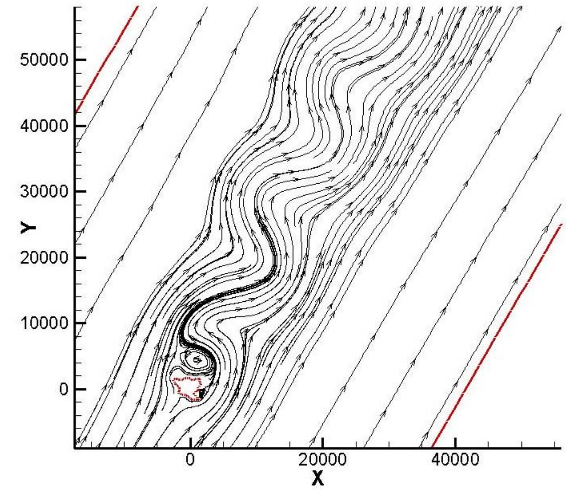

(b)

Fig. 5. Streamline contours of (a) an idealized circular Green island with diameter D = 5 km, and (b) a real geometry of Green island, respectively.

Fig. 6 plots the free-surface manifestation and streamlines of Re = 100 without consideration of Coriolis force. The vortex street can be seen over a distance of about 36 km downstream the island from Fig. 6(a), close to what observed in satellite images, Fig. 3(b) and 3(c), and lose coherent eddy structures further downstream. Fig. 6(b) illustrates the spatial scale of the vortices, where a/b = 3.50 and b/L_r = 1.29, respectively. Fig. 6(c) displays the streamlines. It reveals that flow exits the northeastern open boundary freely, with a minimal reflection.

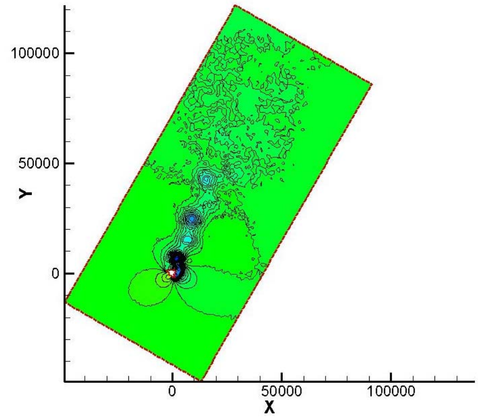

(a)

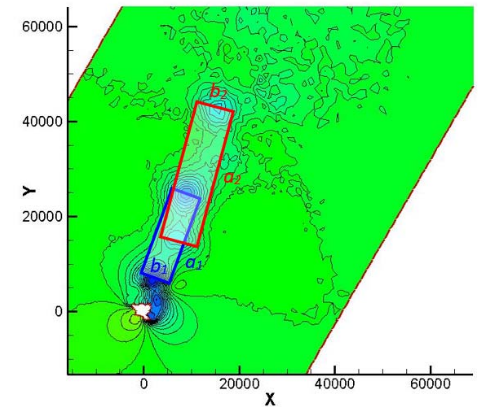

(b)

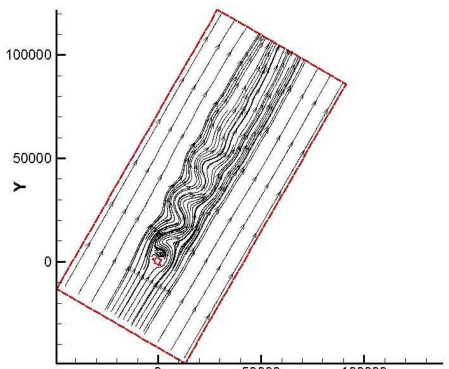

(c)

Fig. 6. (a) Global view and (b) local view of contours of free-

surface, and (c) streamlines of Re = 100 without consideration of Coriolis force.

The vortex shedding is characterized by a well-defined period which is associated with the Strouhal number

$$St = L_r / u_\infty T \qquad (10)$$

where T represents the period of the vortex shedding. Table 1 summaries the eddy properties of Re = 100, 200, and 500, respectively. Values of a/b are in the range of 3.50 to 3.72 and b/L_r 1.29 to 1.33. Therefore, the average value of a/b is 3.63 and b/L_r is 1.31. Relationship of St and Re is plotted in Fig. 7. Computed St of Re = 100 agrees well with the value of $St = 0.2698 - 1.0271/\sqrt{Re}$ proposed by [26], but St of Re = 200 and 500 is underestimated. The underestimation might be attributed to free-surface is not considered in some of the experiment data used for the regression analysis.

The propagation speed of the vortices which defined as $v_e = a/T$ is 0.36-0.51 m/s. This value is in the range of 0.2-0.5 m/s as reported by other literatures [27]. Its magnitude is of the same order as that of the Kuroshio (1.0 m/s), implying the nonlinearity of vortices and interaction of vortices and the Kuroshio is strong.

Fig. 8 depicts the effect of Coriolis force on the eddy dynamics with Re = 100. Fig. 8(a) shows the surface manifestation of eddies. Free-surface on the right-hand side along the main stream is 0.55 m higher than that of the left-hand side. However, slope of the free-surface is very small, about 0.0000076, across the 72,000 m domain width. Comparing the streamlines with consideration of Coriolis force, Fig. 8(b), with that without consideration of Coriolis force, Fig. 5(b), Coriolis force seems to have an insignificant effect on the flow/wake fields.

Table 1. Properties of Green island wake with Re = 100, 200, and 500, respectively.

Re	$Ar = a/b$	$Br = b/L_r$	$St = L_r/u_\infty T$	$u_p = u_e/u_\infty$
100	3.50	1.29	0.17	0.36
200	3.67	1.33	0.18	0.46
500	3.72	1.31	0.20	0.51

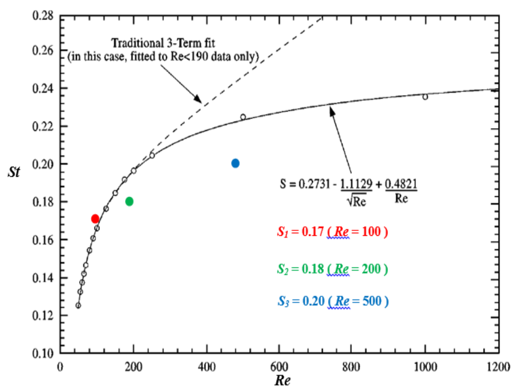

Fig. 7. Comparison of computed St vs. Re with the regression equation of Williamson and Brown (1998).

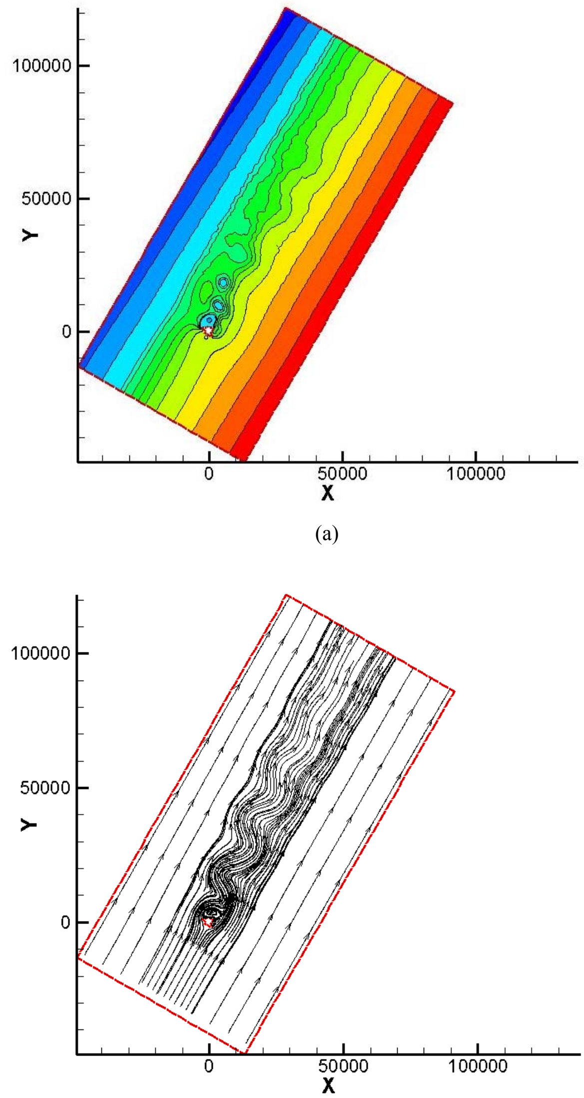

(a)

(b)

Fig. 8. (a) Contours of free-surface and (b) streamlines, respectively, of Re = 100 with consideration of Coriolis force.

V. CONCLUSIONS

Satellite imagery observed wake downstream the Green Island, Taiwan due to passing of the Kuroshio is numerically studied. The theory is based on the depth-averaged shallow-water equations with space-time least-squares finite-element method. Salient features of the vortices, such as the aspect ratio, dimensionless width, the Strouhal number, as well as propagation speed of the vortices for Re = 100, 200, and 500, respectively, are computed and compared with other research results. The results show that the aspect ratio obtained from satellite images is 1.76-2.72 and 3.50-3.72 from numerical modelling. Numerical prediction agrees well with the value of 3.57 resulting from von Kármán's inviscid theory [13]. The dimensionless width is 1.84-1.92 from satellite images and is 1.29-1.33 from numerical simulations. Therefore, computed dimensionless widths are in good agreement with the value of 1.2 from Tyler's laboratory study of flow around a bluff body without free-surface [16].

With numerical model, not only can the spatial scale of the island wake be predicted, the temporal variation of the island wake which unavailable and difficult to assess by the remote sensing technology can be estimated. St is 0.17, 0.18, and 0.20 for Re = 100, 200, and 500, respectively; these values are close to the value reported in [26], see Fig. 7. The propagation speed of the vortices is about 0.31-0.51 m/s which is in the range of 0.2-0.5 m/s reported by previous studies. Effect of Coriolis force on the wake is also conducted and found that Coriolis force does affect the free-surface. However, its influence on eddy properties is insignificant for the small island wake considered.

ACKNOWLEDGMENT

S.-J. Liang is grateful to the National Science Council of Taiwan for Grand ID NSC 100-2221-E-019-004-MY3.

REFERENCES

[1] M. M. Zdravkovich, *Flow Around Circular Cylinder*: *Fundamentals*, vol. 1, Oxford University Press, 1997; *Flow Around Circular Cylinder*: *Applications*, vol. 2, Oxford University Press, 2003.

[2] A. Roshko, On the development of turbulent wakes from vortex streets, *NACA Report 1191*, 1954.

[3] D. J. Tritton, "Experiments on the flow past a circular cylinder at low Reynolds numbers," *Journal of Fluid Mechanics*, 6(4), 1959, pp.547–567.

[4] C. H. K. Williamson, "Vortex dynamics in the cylinder wake," *Annual Review of Fluid Mechanics*, 28, 1996, pp.477–539.

[5] X. Li, P. Clemente - Colón, W. G. Pichel, and P. W. Vachon, "Atmospheric vortex streets on a RADARSAT SAR image," *Geophysical Research Letters*, 27(11), 2000, pp.1655–1658.

[6] G. S. Young and J. Zawislak, "An observational study of vortex spacing in island wake vortex streets," *Journal of Hydraulic Research*, 134(8), 2006, pp.2285–2294.

[7] H.-C. Shen, Topography induced flow variations between Taitung-Lutao off Southeast Taiwan, Institute of Applied Marine Physics and Undersea Technology, National Sun Yat-sen University, Kaoshiung, Taiwan, Master's thesis, 2012.

[8] Y. Jia and Q. Liu, "Eddy shedding from the Kuroshio bend at Luzon Strait," *Journal of Oceanography*, 60(6), 2004, pp.1063–1069.

[9] M.-H. Chang, T. Y. Tang, C.-R. Ho, and S.-Y. Chao, "Kuroshio-induced wake in the lee of Green Island off Taiwan," *Journal of Geophysical Research: Oceans*, 118(3), 2013, pp.1508–1519, doi:10.1002/jgrc.20151.

[10] D. B. Chelton, M. G. Schlax, and R. M. Samelson, "Global observations of nonlinear mesoscale eddies," *Progress in Oceanography*, 91, 2011, pp.167–216.

[11] S.-J. Liang, C.-Y. Lin, T.-W. Hsu, C.-R. Ho, and M.-H. Chang, "Numerical study of vortex characteristics near Green Island, Taiwan," *Journal of coastal Research*, 2013, doi: 10.2112/JCOASTRES-D-12-00245.1.

[12] Q. Zheng, H. Lin, J. Meng, X. Hu, T. Song, Y. Zhang, and C. Li, "Sub-mesoscale ocean vortex trains in the Luzon Strait," *Journal of Geophysical Research*, 113(C4), 2008, C04032, doi:10.1029/2007JC004362.

[13] T. von Kármán and H. Rubach, "Über den mechanismus des flüssigkeits - und luftwiderstandes," *Phys. Z.*, 13(2), 1912, pp.49–59.

[14] R. E. Thomson, J. F. R. Gower, and N. W. Bowker, "Vortex streets in the wake of the Aleutian Islands," *Monthly Weather Review*, 105(7), 1977, pp.873–884.

[15] L. F. Hubert and A. F. Krueger, "Satellite pictures of mesoscale eddies," *Monthly Weather Review*, 90(11), 1962, pp.457–463.

[16] J. Tyler, "A hot wire method for measurement of the distribution of vortices behind obstacles," *Philosophical Magazine*, 9(61), 1930, pp.489–490.

[17] R. S. Johnson, A Modern Introduction to the Mathematical Theory of Water Waves. New York, New York: Cambridge, 1997.

[18] W. Tan, Shallow water Hydrodynamics: Mathematical Theory and Numerical Solution for a Two-Dimensional System of Shallow Water Equations, Elsevier, 1992.

[19] C. B. Vreugdenhil, Numerical Methods for Shallow-Water Flow, Dordrecht, 1994.

[20] Y. Chen, G. Zou, and G. Gong, "An adaptive open boundary condition," *Acta Mechanica Sinica*, 6(4), 1990, pp.305-310.

[21] M. D. Gunzburger, *Finite Element Methods for Viscous Incompressible Flows*. Waltham, Massachusetts: Academic Press, 1989.

[22] T. J. R. Hughes and G. M. Hulbert, "Space-time finite element methods for elastodynamics: Formulations and error estimates," *Computer Methods in Applied Mechanics and Engineering*, 66(3), 1988, pp.339–363.

[23] B. N. Jiang, *The Least-Squares Finite Element Method*. New York, New York: Springer, 1998.

[24] S.-J. Liang, C.-Y. Lan, and Y.-C. Chen, "Shallow water flow modeling using space-time least-squares finite-element method," *Journal of Marine Science and Technology*, 20(5), 2012, pp.595-602, doi: 10.6119/JMST-012-0814-1.

[25] T. E. Tezduyar, M. Behr, S. Mittal, and J. Liou, "A new strategy for finite element computations involving moving boundaries and interfaces – The deforming-spatial-domain/space-time procedure: II. Computation of free-surface flows, two-liquid flows, and flows with drifting cylinders," *Computer Methods in Applied Mechanics and Engineering*, 94(3), 1992, pp.353–371.

[26] C. H. K. Williamson and G. L. Brown, "A series in $1/\sqrt{\mathrm{Re}}$ to present the Strouhal-Reynolds number relationship of the cylinder wake," *Journal of Fluids and Structures*, 12(8), 1998, pp.1073–1085.

[27] L.-Y. Oey, Y.-L. Chang, Y.-C. Lin, M.-C. Chang, F.-H. Xu, and H.-F. Lu, "ATOP – The advanced Taiwan ocean prediction system based on the mpiPOM. Part 1: Model descriptions, analyses and results," *Terrestrial, Atmospheric and Oceanic Sciences*, 24(1), 2013, pp.137–158, doi: 10.3319/TAO.2012.09.12.01(Oc).